Experimental and numerical evaluation of the force due to the impact of a dam-break wave on a structure

Experimental and numerical evaluation of the force due to the impact of a dam-break wave on a structure

FRANCESCA AURELI, PhD, Research Assistant, *Department of Civil and Environmental Engineering and Architecture, University of Parma, Parco Area delle Scienze 181/A, 43124 Parma, Italy*

Email: francesca.aureli@unipr.it

SUSANNA DAZZI, PhD Student, *Department of Civil and Environmental Engineering and Architecture, University of Parma, Parco Area delle Scienze 181/A, 43124 Parma, Italy*

Email: susanna.dazzi@studenti.unipr.it

ANDREA MARANZONI, PhD, Research Assistant, *Department of Civil and Environmental Engineering and Architecture, University of Parma, Parco Area delle Scienze 181/A, 43124 Parma, Italy*

Email: andrea.maranzoni@unipr.it (author for correspondence)

PAOLO MIGNOSA, PhD, Full Professor, *Department of Civil and Environmental Engineering and Architecture, University of Parma, Parco Area delle Scienze 181/A, 43124 Parma, Italy*

Email: paolo.mignosa@unipr.it

RENATO VACONDIO, PhD, Post-doc Researcher, *Department of Civil and Environmental Engineering and Architecture, University of Parma, Parco Area delle Scienze 181/A, 43124 Parma, Italy*

Email: renato.vacondio@unipr.it

Experimental and numerical evaluation of the force due to the impact of a dam-break wave on a structure

ABSTRACT

Flood events caused by the collapse of dams or river levees can have damaging consequences on buildings and infrastructure located in prone areas. Accordingly, a careful prediction of the hydrodynamic load acting on structures is important for flood hazard assessment and potential damage evaluation. However, this represents a challenging task and requires the use of suitable mathematical models. This paper investigates the capability of three different models, i.e. a 2D depth-averaged model, a 3D Eulerian two-phase model, and a 3D Smoothed Particle Hydrodynamics (SPH) model, to estimate the impact load exerted by a dam-break wave on an obstacle. To this purpose, idealized dam-break experiments were carried out by generating a flip-through impact against a rigid squat structure, and measurements of the impact force were obtained directly by using a load cell. The dynamics of the impact event was analyzed and related to the measured load time history. A repeatability analysis was performed due to the great variability typically shown by impact phenomena, and a confidence range was estimated. The comparison between numerical results and experimental data shows the capability of 3D models to reproduce the key features of the flip-through impact. The 2D modelling based on the shallow water approach is not entirely suitable to accurately reproduce the load hydrograph and predict the load peak values; this difficulty increases with the strength of the wave impact. Nevertheless, the error in the peak load estimation is in the order of 10% only, thus the 2D approach may be considered appropriate for practical applications. Moreover, when the shallow water approximation is expected to work well, 2D results are comparable with the experimental data, as well as with the numerical predictions of far more sophisticated and computationally demanding 3D solvers. All the numerical models overestimate the falling limb of the load hydrograph after the impact. The SPH model ensures good evaluation of the long-time load impulse. The 2D shallow water solver and the 3D Eulerian model are less accurate in predicting the load impulse but provide similar results. A sensitivity analysis with respect to the model parameters allows to assess model uncertainty. Finally, the experimental data collected have been made available online as supplementary material for validation purposes.

Keywords: Dam-break; experimental data; hydraulic hazard; impact force; numerical modelling

1 Introduction

Buildings and infrastructure located near dams or river levees can be hit by severe flood events with potentially damaging consequences in the case of collapse of these retaining structures. On the one hand, the presence of construction in the flooding area, along with topographic irregularity, can strongly affect the dynamics of the inundation and the flood's characteristics; on the other hand, violent loads acting on structures can cause serious

damages and even compromise their stability.

A reliable characterization of the fluid-structure interaction is a key task not so much for accurately predicting flood evolution, as for evaluating potential direct damages to structures, defining appropriate failure and damage criteria as well as effective design methods, and planning corrective and preventative measures of damage reduction [24]. Furthermore, the assessment of the capability of structures to withstand flood actions is useful in emergency planning, especially in the case of rapid inundations due to dam-break events, because flood-resistant buildings can guarantee the occupants' safety without the need of evacuation. Hence, in flood risk analysis [61] impact force should be considered as an important parameter, appreciably affecting the hydraulic hazard level. However, the careful prediction of flood actions on structures is a challenging task, especially in the case of violent impact processes, because of the large number of geometric and hydraulic parameters involved ([35], [49]).

Actually, some of these hydraulic quantities (for example, maximum water depth, maximum velocity, flood arrival time, rapidity of the rise, and duration of the flood [4]) are naturally involved, through appropriate combinations, in the formulation of several damage and failure criteria proposed in literature (e.g. [53]). Erpicum et al. [23] employed one of these failure criteria to interactively modify the topography during dam-break simulations. Aureli et al. [6] suggested including maximum total force (thereby accounting for contemporary hydrostatic and dynamic loads) in the set of hydraulic quantities useful for flood inundation modelling and hydraulic hazard assessment. Moreover, on the basis of a dataset concerning a real dam-break event, Gallegos et al. [27] performed structural damage predictions by coupling a hydrodynamic model with a damage model and analyzed the sources of uncertainty associated with the parameters involved.

Mathematical models are indispensable tools for evaluating hydraulic quantities involved in flood hazard analysis and should not only effectively deal with irregular topography, wetting and drying, and transcritical flows, but also accurately predict force actions on structures located in the flow domain. Two-dimensional (2D) shallow water modelling is a widely accepted mathematical tool to simulate rapidly varying open channel flows, even in the presence of obstacles, buildings (either isolated or multiple), and topographical singularities (e.g. [5], [55], [57], [58], [66]) or real bathymetry (e.g. [6], [9], [23], [32], [67]). In this context, if the interest lies in the detailed reconstruction of the near-field flow, a building is usually schematized as a rigid block with impervious walls or, equivalently, as a hole in the computational domain [56]. Otherwise, if a far-field simulation of the flow is sufficient for the purpose of the study, the approaches based on the fictitious strong increment of the friction coefficient [23] or on the concept of porosity of a built-up area ([10], [54], [59]) is used to obtain an overall prediction of the actual effects of these

obstacles on flood propagation. Schubert and Sanders [56] compared different methods to model flood propagation in urban areas on the basis of a real-field dam-break application in order to highlight advantages and drawbacks of the different approaches.

However, it seems obvious to expect that a vertically-averaged approach would show limitations in reconstructing the impact of a dam-break wave against an obstacle, since this phenomenon is locally markedly three-dimensional (3D) and presents strong curvatures of the free surface with non-hydrostatic distribution of pressure along the vertical direction. For this reason, impact processes are usually analyzed in literature by means of 3D numerical models based on Reynolds averaged Navier-Stokes equations integrated by using Eulerian methods (e.g. [1], [37], [70]), SPH (Smoothed Particle Hydrodynamics) Lagrangian methods (e.g. [8], [17], [18], [20], [25]), or hybrid Eulerian-Lagrangian methods [50]. Furthermore, air entrainment effects can also be important in this kind of phenomena, thereby the adoption of a two-phase model is advisable.

This paper aims to compare the capability of 2D shallow water, 3D Eulerian, and 3D Lagrangian models to predict the impact forces caused by a dam-break wave on a structure. The 2D model adopted is a finite volume MUSCL-Hancock scheme based on the weighted surface-depth gradient method (WSDGM) recently proposed by Aureli et al. [7]. The Eulerian 3D model is the FLUENT commercial package, which can handle two-phase flows using the VOF (Volume of Fluid) technique [33]. Meshless Lagrangian 3D modelling is carried out using Dual-SPHysics, a free open-source SPH code specifically developed for free-surface hydrodynamics which solves the Navier-Stokes equations [30]. This software is accelerated by means of the Compute Unified Device Architecture (CUDA), which enables the simulation of violent flows with very high spatial resolution ([2], [68]). Numerical results are compared with data from new physical experiments in order to assess the accuracy of these mathematical models in reproducing an impact process and predicting the associated peak force. A sensitivity analysis on the model parameters is accomplished in order to evaluate the uncertainty associated with the numerical predictions. The main advantages and shortcomings of the three models in this kind of engineering applications are highlighted.

The literature review confirms that experimental studies on this subject have so far mainly dealt with marine and coastal applications (see, for example, [15], [21], [36], [42], [51], [52], [62]), and have been frequently directed towards the design of coastal and off-shore structures. In particular, Lugni et al. [42] investigated the flip-through generated by a sloshing wave by means of a particle image velocimetry technique and highlighted three different modes of the flip-through event according to the breakup features of the approaching wave. The kinematic field and dynamic behaviour were analyzed in detail for each flip-through mode. Later, Lugni et al. ([43], [44]) focused their attention on the flip-through mode characterized by the entrapment of an air cavity in front of the wall. Moreover, several

experimental studies reported in literature concerned debris flow (e.g. [3], [64], [71]), with the aim of both giving insight into the physics of the process and providing recommendations for the design of defence structures. On the other hand, fewer laboratory investigations have been devoted to studying the impact of a dam-break wave against a structure (e.g. [12], [13], [37], [65]), although this topic has recently gained more attention ([16], [41]). The laboratory test case proposed by Yeh and Petroff concerning the impact of a dam-break wave (propagating on wet bed) against a tall structure has been widely employed in literature and is considered a reference for validation purposes ([28], [50]).

A new laboratory investigation was therefore carried out in order to obtain further experimental data for the validation of numerical codes. Since flood waves originated by a total dam failure and propagating in a prismatic channel have mainly been considered in literature, a partial dam-break was induced on dry bed to investigate the frontal collision of the resulting flooding wave against a prismatic obstacle simulating an isolated building. It can certainly be expected that the impact load time series, and in particular the peak load value (which in general is of greater interest for real applications), depends on the shape of the obstacle, on its position and orientation within the flooding area, and on the shape of the impacting wave. However, only the dependence of the peak force on the dam-break initial condition (with reference to the headwater depth) is analyzed in this work.

The net hydrodynamic load exerted by the wave on the structure was measured by means of a load cell able to compensate errors due to off-centre forces. In this way an integral measurement of the dynamic interaction between fluid and structure is directly provided (see, for example, [12], [13], [52]). Since the designers' practical interest is often focused on the evaluation of the total force (possibly associated with its probability of occurrence), this measuring technique is preferable to the one based on the integration of multiple simultaneous pressure measurements obtained from several transducers mounted on a wall (as in [14], [16], [42] and [60], for example). Moreover, several experimental studies in literature have shown that pressure measurements obtained during very strong impacts are typically highly scattered, thus impact force appears more suitable than impact pressure to assess the effectiveness of numerical models in the framework of impact wave problems.

The paper is structured as follows. The experimental set-up is detailed in Section 2, whereas the three numerical models are presented in Section 3. In Section 4 a typical observed load time history is linked to the phases of the impact physics, and a repeatability analysis is carried out in order to assess the reliability of the experimental data. The consistency of the load impulse in characterizing the wave impact is also discussed. Finally, experimental data and numerical results are compared, and the predictive capability of the numerical models is assessed also on the basis of a sensitivity analysis on the model parameters.

2 Experimental set-up

Experiments were carried out at the Hydraulics Laboratory of Parma University in the set-up sketched in Fig. 1. The facility consisted in a 2.60 m long and 1.20 m wide rectangular Plexiglas tank divided into two compartments – a 0.80 m × 1.20 m upstream reservoir, and a downstream flood plain – by means of a separating wall equipped with a 0.30 m wide gate placed in the middle. The bottom of the experimental facility was horizontal. The gate moved upward and could be quickly opened by means of a simple manhandled pulley system.

A prismatic block with rectangular section and vertical walls was placed in the flood plain just in front of the gate (0.51 m downstream) with the aim of representing an isolated building. This obstacle was 0.30 m wide, 0.155 m thick and 0.20 m tall, and was realized by means of a PVC box structure reinforced with aluminium sheets. In this way, the resulting element was at the same time very rigid and sufficiently lightweight to reduce inertia.

In order to measure the net hydrodynamic force acting on the obstacle in the *x*-direction, the box was equipped with a load cell inside, fixed with a squat metallic cantilever-beam on a very stiff support system placed above. This contrasting structure was specifically designed in such a way that the box was hanging a few tenths of a millimetre above the bottom of the facility; as a consequence, the impact force was entirely transmitted to the load cell. The force-measuring device was a DS Europe EG-A1 transducer, based on a parallelogram flexure, sensitive exclusively to compression forces with full scale of about 30 N. Due to their specific operating principle, this kind of devices is suitable for dynamic measurements. Moreover, the load cell was able to compensate the effects induced by a decentred force applied to a squared area of 0.40 m × 0.40 m. The output signal from the load cell was sampled at the frequency of 1 kHz by using a NI USB-4432 data logger with 24 bit resolution and then filtered *a posteriori* by a numerical low-pass 5^{th} order Butterworth filter with 50 Hz cut frequency. Static sensitivity of 0.317 V/N was found from static calibration and total inaccuracy was estimated to be approximately 0.10% of full scale. The threshold force due to internal friction between the different components of the measuring system was estimated equal to 1.85 N. Calibration of the dynamic characteristics of the load cell showed a step response typical of an underdamped second-order system. The 10% settling time (which can be considered an effective indicator of the speed of response [22]) was estimated equal to 0.10 s after the application of a step input.

The acquisition time was synchronized with the gate opening through the motion-induced abrupt variation in the output signal of a photocell. The removal of the gate (with reference to a stroke of 0.10 m) was performed in about 0.08 s, as proved by high-speed video recording; consequently, the release process can be considered instantaneous according to the empirical criterion proposed by Lauber and Hager [39].

During the preparation of each experiment, the water surface was measured at the observation point G1 shown in Fig. 1 by using a 0.5 mm accurate Banner S18U ultrasonic transducer, in order to achieve the initial still-water depth desired in the reservoir. Finally, the impact process was filmed from a lateral viewpoint for different test conditions using a high speed digital video camera able to acquire 100 frames per second with 1,280 × 720 resolution.

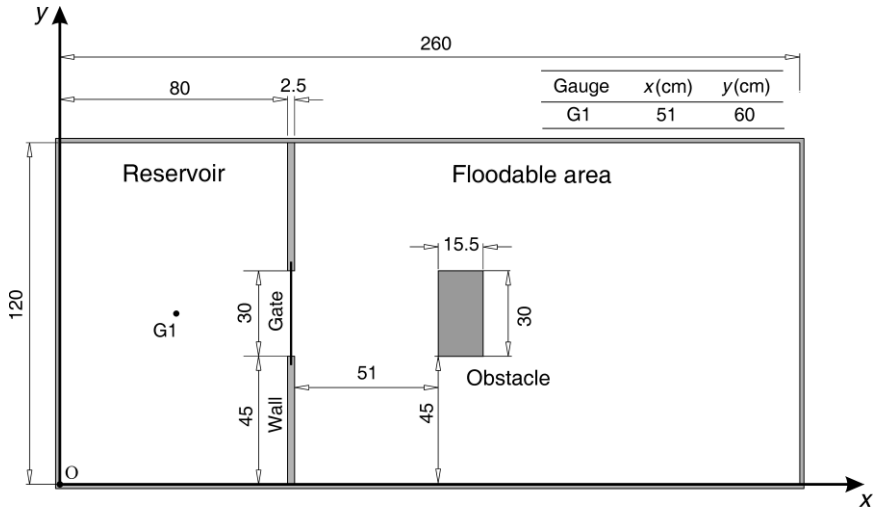

Fig. 1. Plan view sketch of the experimental set-up (measures in cm). G1 indicates a water surface gauge.

3 Numerical models

This section presents the main features of the mathematical models employed to reproduce the experimental impacts and estimate the hydrodynamic load exerted by a dam-break wave on the structure.

Because of the violence of the wave impact observed during the experiments and the expected preponderance of inertial effects, the flow was assumed incompressible according to Cooker and Peregrine [19]. The obstacle was modelled as infinitely rigid neglecting the elastic response of the contrasting structure.

3.1 2D shallow water

The dam-break experiments were first simulated using a finite volume numerical solver based on 2D shallow water equations (e.g. [63]), not including viscosity and turbulence effects.

It is well known that the integral form of 2D shallow water equations reads:

$$\frac{\partial}{\partial t}\int_A \mathbf{U}\, dA + \int_\Omega \mathbf{H}\cdot\mathbf{n}\, dC = \int_A \left(\mathbf{S}_0 + \mathbf{S}_f\right) dA, \tag{1}$$

where A is the surface of the 2D integration element, Ω the element boundary, $\mathbf{n}$ the outward unit vector normal to Ω, $\mathbf{U}$ the vector of the conserved variables, and $\mathbf{H} = (\mathbf{F}, \mathbf{G})$ the tensor of fluxes in the x and y directions with

$$\mathbf{U} = \left[h;\quad uh;\quad vh\right]^T,\ \mathbf{F} = \left[uh;\quad u^2h + \tfrac{1}{2}gh^2;\quad uvh\right]^T,\ \mathbf{G} = \left[vh;\quad uvh;\quad v^2h + \tfrac{1}{2}gh^2\right]^T. \tag{2}$$

Here h is the flow depth, u and v are the velocity components in the x and y directions respectively, and g is the acceleration due to gravity. The bed and friction slope source terms $\mathbf{S}_0$ and $\mathbf{S}_f$ are expressed according to the following definitions:

$$\mathbf{S}_0 = \left[0;\quad -gh\frac{\partial z}{\partial x};\quad -gh\frac{\partial z}{\partial y}\right]^T,\ \mathbf{S}_f = \left[0;\quad -gh\frac{n_f^2\, u\sqrt{u^2+v^2}}{h^{4/3}};\quad -gh\frac{n_f^2\, v\sqrt{u^2+v^2}}{h^{4/3}}\right]^T, \tag{3}$$

where z denotes the bed elevation with respect to a horizontal reference, and n_f the Manning coefficient.

Finite volume schemes allow to compute the variation $\Delta\mathbf{U}$ of the cell-averaged conserved variable in the time interval Δt as a function of the forcing source terms and of the numerical fluxes exchanged through the boundaries. If applied to a grid composed of quadrangular elements, the System of equations (1) assumes the fully discrete form [63]:

$$\Delta\mathbf{U} = -\frac{\Delta t}{\mathcal{A}}\sum_{k=1}^{4}\left(\mathbf{f}_k\cdot\mathbf{n}_k\right)\Delta l_k + \frac{\Delta t}{\mathcal{A}}\int_A \left(\mathbf{S}_0 + \mathbf{S}_f\right) dA \tag{4}$$

in which $\mathcal{A}$ is the area of the grid cell, $\mathbf{f}_k$ represents the numerical fluxes exchanged through the boundaries between neighboring cells, and $\mathbf{n}_k$ is the outward unit vector normal to the k-side (of length Δl_k) of the computational cell.

The evaluation of numerical fluxes was performed through the Weighted Surface-Depth Gradient Method (WSDGM) proposed and tested by Aureli et al. [7]. A 5 mm square mesh was used. Stability constraint was introduced by assuming the Courant number equal to 0.9. For the laboratory facility here considered, based on a suitable calibration Aureli et al. [5] recommended to set the Manning coefficient at 0.007 s $m^{-1/3}$.

The intensity of the net force acting on the obstacle in the x-direction (perpendicular to the vertical wall facing the gate) was estimated by using three different methods:

(1) the first consists in summing up, time step by time step, the "total force" (sum of hydrostatic load and momentum flux term) calculated for each cell adjacent to the two walls normal to the x-direction; if the computational mesh is Cartesian with size

$\Delta x \times \Delta y$ and the solid wall is parallel to the y-axis (along the column i, from j_1 to j_2 line), at the time level n:

$$F^n = \sum_{j=j_1}^{j_2} \rho g \frac{(h_{i,j}^n)^2}{2} \Delta y + \rho \frac{(uh_{i,j}^n)^2}{h_{i,j}^n} \Delta y, \quad (5)$$

with ρ representing the density of water;

(2) the second is based on the application of the linear momentum equation (projected in the x-direction) to the mesh elements adjacent to the two walls normal to the x-direction; this method leads to:

$$F^n = \sum_{j=j_1}^{j_2} F^n_{i+\frac{1}{2},j}, \quad (6)$$

where $F_{i+1/2,j}$ is the static load at the $(i+1/2, j)$ solid boundary, which can be evaluated as follows:

$$F^n_{i+\frac{1}{2},j} = \rho \frac{uh_{i,j}^n - uh_{i,j}^{n+1}}{\Delta t} \Delta x \Delta y + \rho (f_2)^n_{i-\frac{1}{2},j} \Delta y - \rho \left[(g_2)^n_{i,j+\frac{1}{2}} - (g_2)^n_{i,j-\frac{1}{2}} \right] \Delta x - \rho g h_{i,j}^n (S_{f_x})_{i,j}^n \Delta x \Delta y, \quad (7)$$

where f_2 and g_2 are the second vector components of the numerical fluxes **f** and **g,** respectively;

(3) the final one consists in applying the linear momentum equation (projected in the x-direction) to a suitable rectangular control volume including the obstacle (sized 75.5 cm × 90 cm and centred around the block in the application here described).

A short comment on the comparison of the results obtained from the methodologies described above is provided in Section 4.3.

3.2 3D Eulerian

Three-dimensional simulations of the dam-break experiments were performed using FLUENT, widespread commercial software for computational fluid dynamics [26] based on the finite volume (FV) discretization.

The flow was modelled as an incompressible and immiscible two-phase system (water-air) adopting the Volume of Fluid (VOF) approach implemented in the FLUENT solver and including the effect of surface tension (even if likely not relevant in wave impact problems, according to Peregrine [49]).

The governing equations are the Reynolds-averaged conservation equations for mass and momentum, which for a homogeneous incompressible flow can be written as follows:

$$\nabla \cdot \overline{\mathbf{v}} = 0; \quad \frac{D\overline{\mathbf{v}}}{Dt} = \mathbf{g} - \frac{1}{\rho}\left(\nabla \cdot \overline{\mathbf{T}} + \nabla \cdot \overline{\mathbf{T}}_R\right), \tag{8}$$

where the overbar denotes the time averaged value of the current variable, **v** represents the fluid velocity, **g** the body forces per unit of mass, **T** the stress tensor, and $\mathbf{T}_R$ the Reynolds stress tensor. According to the VOF approach, the equation of the volume fraction for a two-phase system is:

$$\frac{\partial C}{\partial t} + \nabla \cdot \left(\mathbf{v}\, C\right) = 0 \tag{9}$$

where C is the volume fraction of one of the two fluids (water). The volume fraction function is used as a weighting factor to obtain volume-averaged fluid properties in each computational cell; for example, for the density:

$$\rho = C\rho_w + (1 - C)\rho_a\,, \tag{10}$$

where ρ_w and ρ_a are the density of water and air, respectively.

The bounded second order central differencing scheme was chosen to solve the governing equations. The Large Eddy Simulation (LES) model coupled with Smagorinsky's subgrid-scale model was adopted to simulate the effect of turbulence according to LaRocque et al. [38], who showed that LES model is more suitable than the classic Reynolds Averaged Navier-Stokes (RANS) equations with k-ε turbulence model in predicting dam-break propagation on a dry bed.

The mesh was created using quadrangular elements having 15 mm mean size and a suitable inflation was introduced close to the solid walls with 1 mm near-wall resolution. A refinement based on grid elements of about 10 mm face size was restricted to a 45.5 cm × 60 cm computational area including the obstacle in order to better resolve the computational zone involved in the flip-through process. The resulting mesh consisted in a total of almost 385,000 elements. All boundaries of the computational domain were assumed to be rigid walls except for the top boundary, where a pressure outlet at constant atmospheric pressure was imposed. The initial condition was defined by specifying the presence of water at rest in the reservoir (up to a fixed level) and of air elsewhere. A fixed computational time step of $0.5 \cdot 10^{-3}$ s guaranteed the numerical stability of the computations.

The overall force acting on the obstacle in the longitudinal direction was calculated by integrating the static pressure distributions over the two walls normal to the x-direction and neglecting the effect of shear stresses on the lateral faces of the structure.

3.3 3D SPH

The main features of the 3D Smoothed Particle Hydrodynamics (SPH) model here used are

presented in Gómez-Gesteira et al. [30].

The fundamental principle of SPH method is to approximate any function $A(\mathbf{r})$ by:

$$A(\mathbf{r}) = \int A(\mathbf{r}')W(\mathbf{r}-\mathbf{r}', h)\,d\mathbf{r}\,, \tag{11}$$

where h is the smoothing length, $W = W(\mathbf{r} - \mathbf{r}', h)$ the weighting function or kernel, and $\mathbf{r}$ the position vector. In discrete notation this assumption leads to the following approximation of the function at the generic particle (interpolation point) a:

$$A(\mathbf{r}_a) = \sum_b m_b \frac{A_b}{\rho_b} W_{ab}\,, \tag{12}$$

where the summation is extended to each particle b within the region of the compact support of the kernel function. Mass and density for particle b are denoted by m_b and ρ_b respectively, and $W_{ab} = W(\mathbf{r}_a - \mathbf{r}_b, h)$ denotes the corresponding value of the weight function. The classic third-order cubic spline kernel was adopted in this work [40].

The mass and momentum conservation equations written in Lagrangian form read:

$$\frac{D\rho}{Dt} = -\rho\nabla\cdot\mathbf{v}; \quad \frac{D\mathbf{v}}{Dt} = -\frac{1}{\rho}\nabla p + \mathbf{g} + \Theta\,, \tag{13}$$

where $\mathbf{v}$ is the velocity vector, p is the pressure, and Θ refers to the viscous diffusion term. The SPH scheme herein applied considers water as a weakly compressible fluid. Thus governing equations (13) are coupled with the classic stiff equation of state:

$$p = B\left[\left(\frac{\rho}{\rho_0}\right)^{\gamma} - 1\right], \tag{14}$$

where ρ_0 is the reference density, γ is a dimensionless parameter typically assumed equal to 7, and $B = c_0^2\rho_0\,\gamma^{-1}$, in which c_0 represents the speed of sound at the reference density. Due to the Courant-Friedrichs-Levy stability condition, the computational time steps calculated on the basis of the real speed of sound are too small, thus leading to extremely high computational costs. For this reason, c_0 was restricted to be approximately one order of magnitude greater than the maximum fluid velocity expected; in spite of this approximation, density variations are smaller than 1% and accurate results can be obtained.

According to the SPH method, Equations (13) are discretized as follows:

$$\frac{d\rho_a}{dt} = \sum_b m_b(\mathbf{v}_a - \mathbf{v}_b)\cdot\nabla_a W_{ab}; \quad \frac{d\mathbf{v}_a}{dt} = -\sum_b m_b\left(\frac{P_b}{\rho_b^2} + \frac{P_a}{\rho_a^2} + \Pi_{ab}\right)\nabla_a W_{ab} + \mathbf{g}\,, \tag{15}$$

where Π_{ab} is the viscosity term that in this work is expressed using the classic artificial viscosity formulation [29]:

$$\Pi_{ab} = \begin{cases} \dfrac{-\alpha c_0 \mu_{ab}}{\rho_{ab}} & \text{if } \mathbf{v}_{ab}\cdot\mathbf{r}_{ab} < 0 \\ 0 & \text{if } \mathbf{v}_{ab}\cdot\mathbf{r}_{ab} \geq 0 \end{cases} \quad \text{with } \mu_{ab} = \frac{h\,\mathbf{v}_{ab}\cdot\mathbf{r}_{ab}}{\mathbf{r}_{ab} + 0.01h^2}\,, \tag{16}$$

where $\mathbf{r}_{ab} = \mathbf{r}_a - \mathbf{r}_b$ and $\mathbf{v}_{ab} = \mathbf{v}_a - \mathbf{v}_b$, being $\mathbf{r}_k$ the position vector of the generic particle k and α a free parameter set equal to 0.15. Moreover, the density diffusion term proposed by Marrone et al. [45] was added to the continuity equation to increase the accuracy in density calculation and reduce numerical noise in the pressure field.

The dynamic boundary particles method was adopted for the treatment of the solid boundary conditions. According to this approach, the walls of the obstacle are discretized by means of a set of "structure particles" that satisfy the same equations as the fluid ones, but with unchanged positions. This guarantees that complex domains can be easily reproduced and leads to a good compromise between accuracy and computational costs. The correction proposed by Huges and Graham [34] was also applied to avoid unphysical clumping of fluid particles near the walls. Integration in time was performed using the Sympletic method and velocity was corrected according to the XSPH formulation [46].

A particle resolution of 2.5 mm was used in the numerical simulations. The Courant number was set at 0.2 according to the stability analysis for weakly compressible SPH schemes ([47], [48], [69]).

Finally, numerical force was computed by integrating the pressure distribution on the structure particles located at the front walls of the obstacle (normal to the x-direction). The contribution due to the shear stresses acting on the lateral surfaces was assumed to be negligible.

4 Experimental observations and numerical results

Several tests were performed in different test conditions characterized by initial still-water depth h_u in the reservoir within the range 7–13 cm. This range allowed to meet two opposite requirements: (i) the dam-break impact against the obstacle had to be sufficiently strong to induce a measured force significantly greater than the threshold of the measuring system, but, at the same time, (ii) it could not be too violent so as to prevent wave overtopping. The flood plain was assumed to be initially dry in all tests ($h_d = 0$ m).

Experimental data and numerical results are presented and compared in this section.

4.1 Physical description of the phenomenon

Fig. 2 shows some significant video frames concerning the impact process which occurred during one of the experimental runs carried out with reference to the initial condition of $h_u = 0.10$ m and $h_d = 0$ m. Methylene blue (acting as a light absorber) was dissolved in water with the aim of improving image readability. The experimental points corresponding to the selected stages represented in the images of Fig. 2 are indicated in Fig. 3 over the measured load hydrograph, in order to relate the main features of the impact force time history to the

physical evolution of the phenomenon. Since the main interest is focused on the impact dynamics, the load hydrograph of Fig. 2 is restricted to the first 3 s after the gate removal.

After the breach opening, the flooding wave freely spreads over the initially dry downstream area (frame I1) and reaches the obstacle approximately at time $t = 0.36$ s. Frame I2 captures one of the very first stages of the wall impact, whereas the following images I3 and I4 show details of the progress of the collision process. An upward-moving jet forms at the wall, flipping up in front of the approaching dam-break wave (frame I3). According to Cooker and Peregrine [19], this impact is of "flip-through" type: the wave, in some way, climbs up along the wall ([16], [42]). No air is entrapped between the wall and the jet, which is distinctive of the mode (a) flip-through event defined in Lugni et al. [42]. This typical collision mechanism ensues from an incoming wave dominated by inertia [3] and usually generates very high pressures (e.g. [11], [31]) acting during very short timescales [49]. The sudden upward deviation of the flow is associated with strong accelerations which produce high pressure gradients especially on the toe of the obstacle and, consequently, an abrupt increase in the overall impact force. When the run-up jet, decelerated by gravity, reaches its maximum elevation, it breaks up (frame I4) and starts to detach from the vertical wall overturning backward (frame I5). The maximum value of impact load is achieved precisely at this later stage ($t = 0.71$ s). The falling jet then collapses onto the water surface of the incoming dam-break wave creating an entrapped cavity (frame I6). The splash up of the plunging jet on the back flow creates new surges that rebound on the water surface (frame I7) producing a strong surface mixing with air entrapment. This phenomenon causes a new increase in pressure stresses and, consequently, in the force acting on the obstacle. The measured force shows another peak value, but less severe and shorter in time than the previous one (frame I8). Then, a stable shock wave develops in front of the obstacle (frame I9). The front of this wave is rather disturbed and the jump in water depth is associated with turbulence, entrainment of air pockets, and irregular pulsations which produce undulations in the falling limb of the load hydrograph.

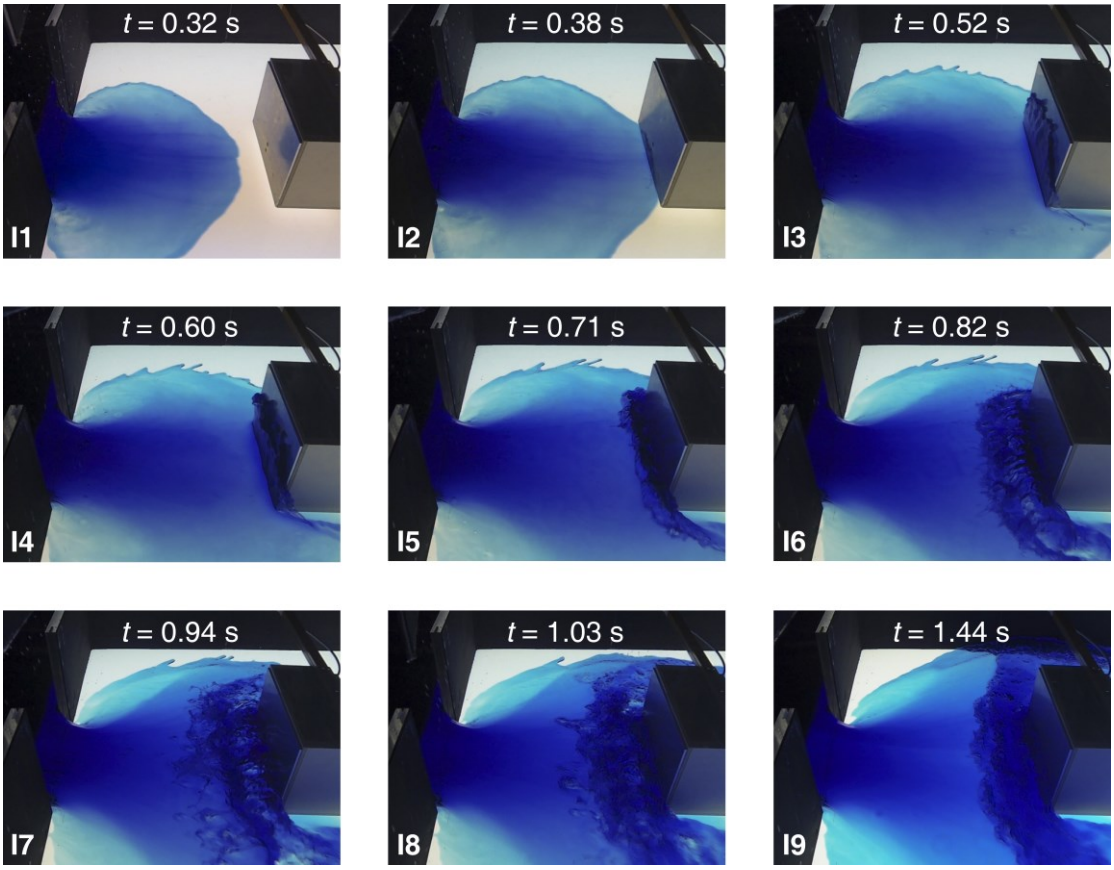

Fig. 2. Sequence of video images concerning a typical impact process of "flip-through" type.

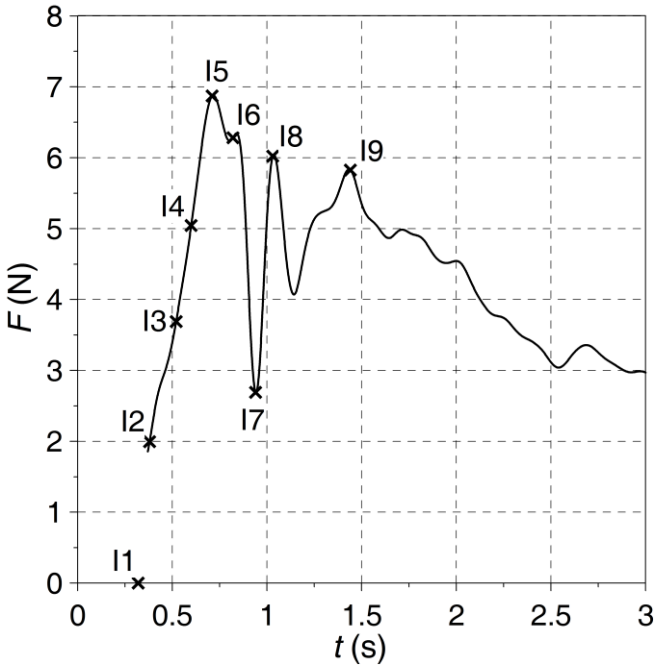

Fig. 3. Typical record of impact total force versus time (crosses highlight hydrodynamic loads exerted on the obstacle at the times of the frames presented in Fig. 2).

The observed phenomenon was simulated by using the numerical models presented in Section 3. Fig. 4 shows some 2D numerical results at three of the times considered in Fig. 2. Obviously, the complex dynamics of the flip-through impact cannot be reproduced by a 2D shallow water model. The formation of a hydraulic jump in front of the obstacle is predicted in the simulated flow with a maximum water depth of approximately 7 cm. On the other hand, both 3D numerical models are able to reproduce the overall dynamics of the phenomenon (Figg. 5 and 6).

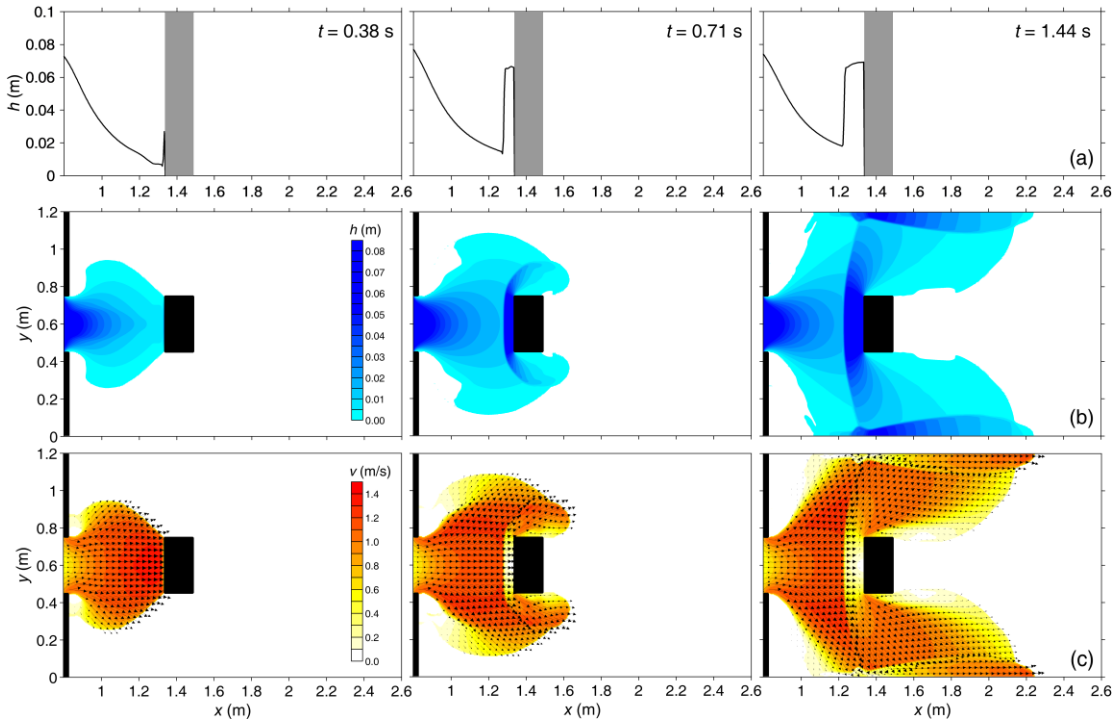

Fig. 4. Example of numerical results obtained from the 2D shallow water model: (a) longitudinal water level profiles at $y = 0.6$ m, (b) water depth contour maps, (c) vector maps of the velocity field along with velocity magnitude contour maps at $t = 0.38$ s, $t = 0.71$ s, and $t = 1.44$ s.

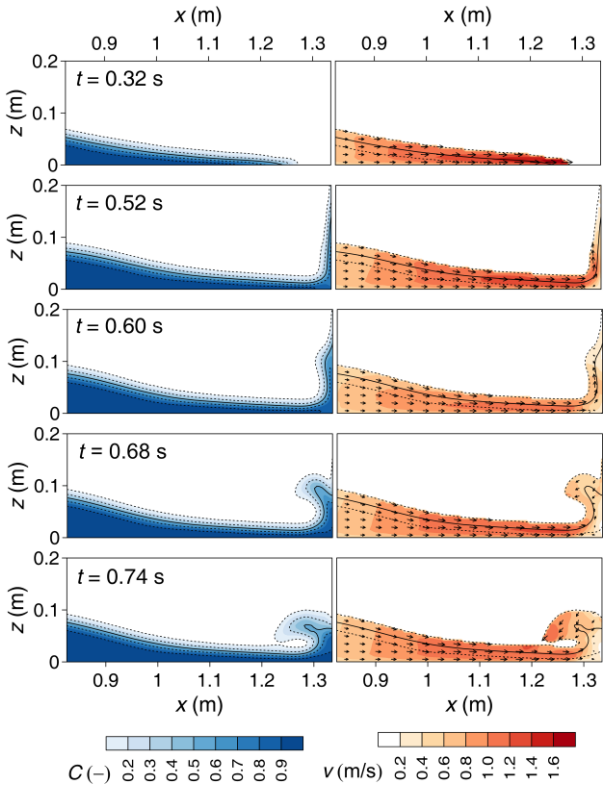

Fig. 5. Example of numerical results returned by FLUENT: contour maps of the volume fraction of water (left) and of the velocity field (right) along the longitudinal plane of symmetry during the first stages of the impact.

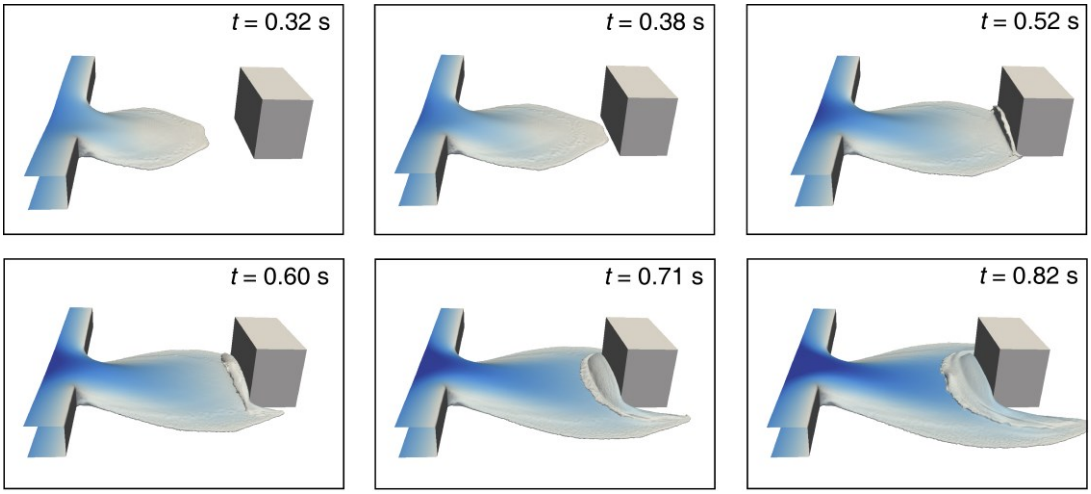

Fig. 6. Snapshots of the dam-break simulation accomplished by the 3D SPH model.

4.2 Repeatability analysis

Experimental observations in literature have proven that impact phenomena systematically show great variability, even if deriving from nominally identical physical conditions (e.g. [49]). Indeed, impact modes can be assumed to differ in each experiment due to poor

repeatability of the gate removal procedure and different propagation of the dam-break front approaching the obstacle induced by 3D effects.

A repeatability analysis was therefore carried out with the aim of assessing the reliability of the measured hydrodynamic load data: 40 runs were repeated under the same test conditions (h_u = 0.10 m, h_d = 0 m) and the experimental data were compared. Fig. 7 shows an example of comparison between measured load data obtained (for $t \leq 3$ s) during two different runs (no. 1 and no. 8). The scatter plot shows some dispersion around the reference bisecting line (Fig. 7b); an overall measurement of the difference between the two load time series is provided by the root-mean-square deviation, which, in this case, is equal to 0.37 N. In particular, the more notable discrepancy between the two load time series occurs in the second peak at about 1 s (Fig. 7a), due to the complex phenomenon induced by the collision of the plunging jet at the wall on the incoming flow.

If the contemporary load data extracted from each of the 40 runs are assumed to have a Gaussian distribution, a confidence range can be estimated, within which the true load time history can be expected to lie with assigned confidence level (see Section 4.3 for details). Moreover, since the peak values of the 40 experimental load time histories are approximately simultaneous, it can be reasonably hypothesized that even these extreme values are normally distributed too. Fig. 8, which compares sample and theoretical values of the cumulative frequency function by means of a probability chart, qualitatively shows the conformity of the Gaussian distribution to the maximum data observed. A summary of this statistical analysis is presented in Table 1, which reports maximum impact forces $F_{\max \beta}$ of different probabilities β.

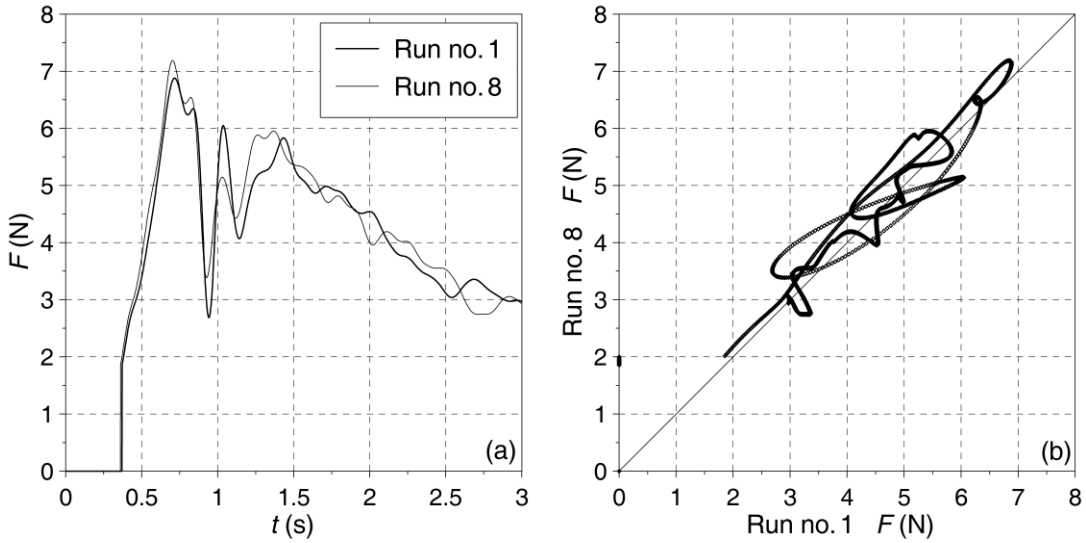

Fig. 7. Comparison between measured load data concerning two different test runs characterized by the same initial condition (h_u = 0.10 m): (a) time history; (b) scatter plot.

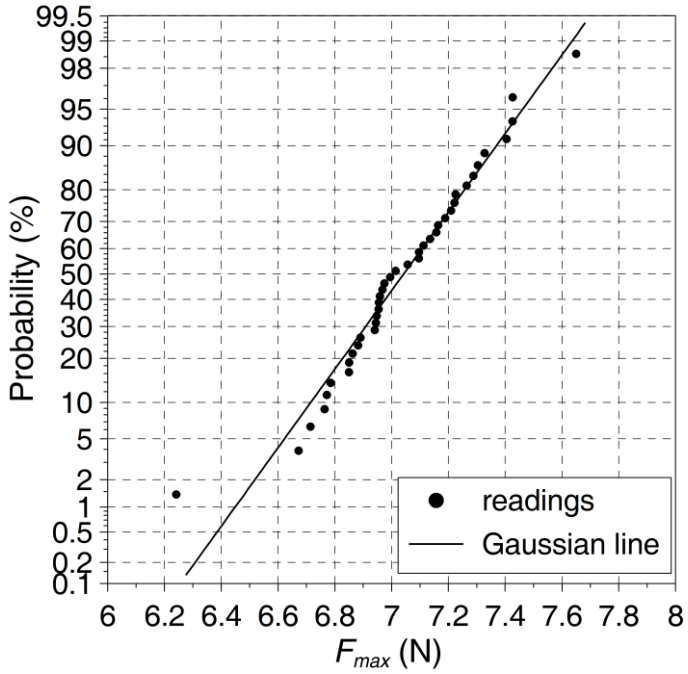

Fig. 8. Graphical check of the suitability of Gaussian distribution to describe the empirical cumulative distribution function of peak load values for h_u = 0.10 m (40 readings with sample mean value equal to 7.04 N and sample standard deviation equal to 0.255 N).

Table 1

Maximum impact forces of different probabilities for the test cases characterized by h_u = 0.10 m.

β	99%	95%	50%	5%
$F_{\max\,\beta}$ (N)	7.63	7.46	7.04	6.62

A meaningful alternative representation of the evolution in time of the impact process is commonly provided by using force impulse as variable of interest. Load impulse is defined in literature (see for example [20]) as the integral in time of the time-varying force and quantifies the overall linear momentum absorbed by the structure starting from the initial time t = 0 up to the actual time t. In general, load impulse globally shows greater repeatability compared to the impact force [49]. The consistency of load impulse in characterizing the wave impact is confirmed by the experimental impulse time histories represented in Fig. 9.

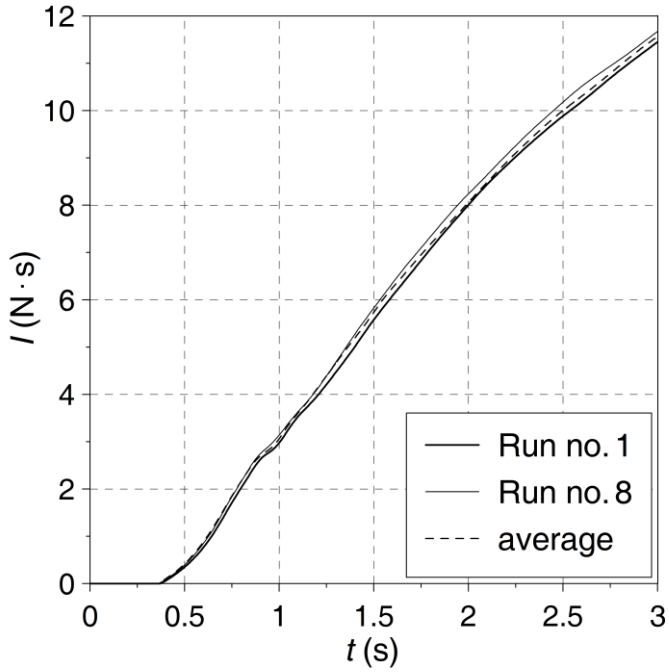

Fig. 9. Comparison between experimental load impulse concerning two different test runs characterized by the same initial condition (h_u = 0.10 m). The dashed line represents the average impulse time history derived from 40 experimental runs.

4.3 Impact load time history

In Fig. 10 the computational impact load time histories are compared with experimental data for the reference test case with h_u = 0.10 m. The gray band represents a 90% confidence interval of the observed data; the upper and lower limits are identified by 95% and 5% percentile levels respectively, estimated on the assumption that contemporary load data obtained from the repeatability analysis have a Gaussian distribution. The time series of the mean values is also reported. The analysis is restricted to the time interval $t \leq 3$ s; in this time range the dam-break wave surely acts on the frontal vertical wall only. Actually, the force acting perpendicularly to the most exposed wall generally is the quantity of main interest for practical applications. The experimental occurrence time of impact (that is the time interval that the incident wave needs to reach the obstacle) is approximately 0.36 s and shows good repeatability (confirmed by a standard deviation of $5 \cdot 10^{-3}$ s), although the gate removal duration is of the same order of magnitude. After the first stages of the impact and the formation of a stable shock wave in front of the wall, load values decrease and the confidence interval reduces in width.

It is well known that 2D shallow water approximation derives from the key assumption that vertical accelerations are negligible. Therefore, it is expected that the shallow water approach is unable to reproduce the first stages of the impact process and predict the "church roof" profile [49] shown by the experimental data. In fact, the peak value of the load

time history is slightly underestimated by the 2D numerical model, while the peak load time is delayed. Anyhow, the arrival time of the dam-break wave at the obstacle is correctly reproduced and the numerical load decaying with time, which occurs in the interval $1.5\ \text{s} < t < 3\ \text{s}$, shows a falling trend that agrees reasonably well with the experimental one, even if load values are slightly overestimated. This part of the load hydrograph is due to the formation of a reflected wave for which the hypothesis of hydrostatic pressure is realistic. It is to be noted that the three methodologies presented in Section 3.1 for evaluating impact force lead to almost identical results: for the test case considered with mesh size $\Delta x = \Delta y = 5$ mm, within the time interval $t \leq 3$ s the root-mean-square deviation between the numerical hydrographs obtained using methods (1) and (2) is equal to $8.8 \cdot 10^{-2}$ N, whereas it is $13.4 \cdot 10^{-2}$ N using methods (1) and (3). For this reason, only the results returned by the method (1) based on Eq. (5) are shown in the following.

Fig. 10 highlights that, as expected, 3D numerical results show better agreement with the experimental data in the first stages of the impact process. The characteristic double-peak trend is captured by the 3D finite volume (FV) model: the first peak is accurately predicted (even if slightly anticipated), whereas the second peak is fairly overestimated. Actually, due to its capability of dealing with two-phase flows, the 3D Eulerian solver can predict the pressure field which arises into the big air pocket that forms in front of the wall in consequence of the fall of the flip-through jet (Fig. 2, frames I6–I8). However, if the compressibility of trapped air is neglected, the air cushion effect expected ([17], [49]) cannot be reproduced, with consequent overestimation of the secondary peak force. Moreover, an evident tendency to overestimation can be observed in the falling limb of the load hydrograph, which also shows strong fluctuations in the interval $2\ \text{s} < t < 3\ \text{s}$, probably due to both the complexity of the biphasic two-phase flow field induced by the wave impact and the difficulty of correctly reproducing the air entrainment effects.

According to the SPH model, the front propagates more slowly towards the obstacle, since the impact time is slightly delayed. Moreover, the model predicts two load peaks which appear underestimated and closer in time compared to the experimental ones. The reason for this discrepancy could be sought for in both the numerical treatment at the reflective boundary and the low spatial resolution of the pressure distribution evaluated at the wall interface due to the particle spreading consequent to the gate release. The predicted falling limb is overestimated, but the global trend matches the experimental results.

All the numerical simulations overestimate the impact load within the time range $1.5\ \text{s} < t < 3\ \text{s}$, after the first stages of the impact process. According to Raad and Bidoae [50], this fact could be explained by considering that the splash up of the plunging jet on the

approaching flow causes a significant entrainment of air pockets with consequent local decrease in the fluid density.

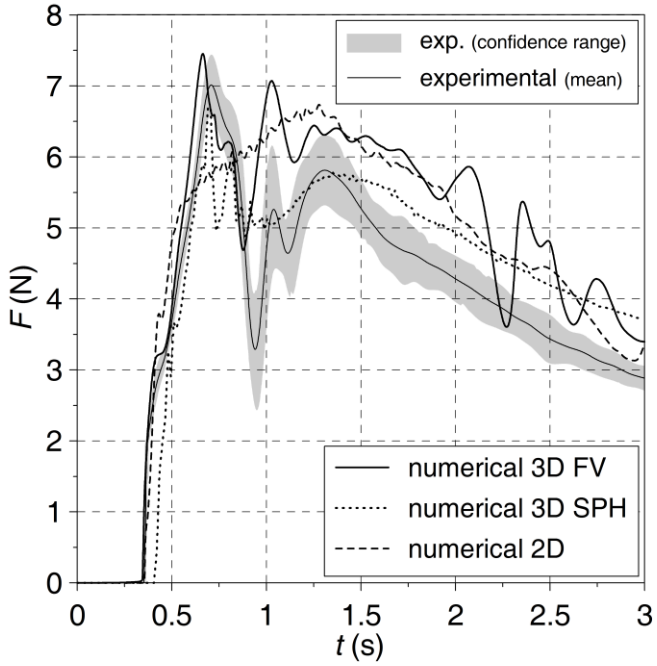

Fig. 10. Comparison between experimental and numerical load time histories. The gray band represents the 90% confidence interval of the data observed (95% and 5% percentile levels being the upper and lower confidence limits, respectively).

Fig. 11 compares the numerical load impulse time histories with the experimental one computed on the basis of the mean load values represented in Fig. 10. The two sets of numerical results obtained from 2D shallow water and 3D Eulerian models match well. However, both models tend to overestimate the overall linear momentum transmitted to the structure if durations greater than 1 s are considered. The load impulse time series predicted by the SPH model instead tracks the experimental data better; the slight underestimation that occurs in the first stages of the impact for durations shorter than 2 s is mainly attributable to the delay characterizing the impact time.

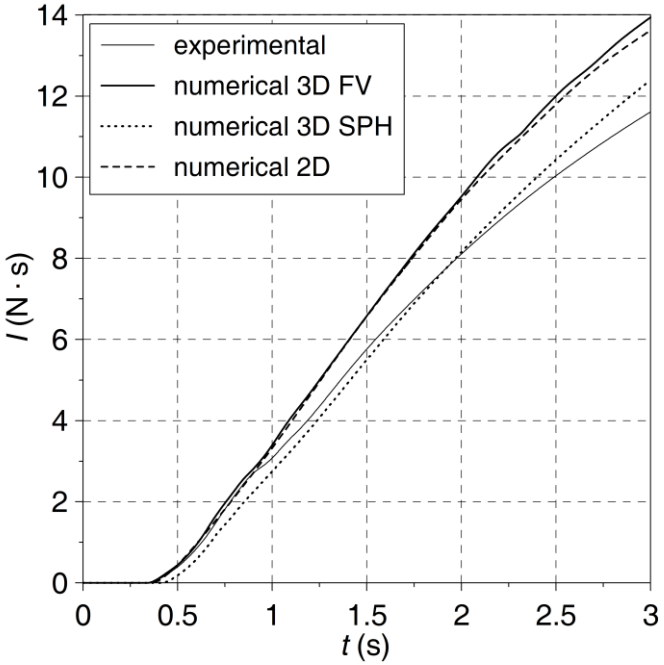

Fig. 11. Comparison between experimental and numerical load impulse time histories.

4.4 Sensitivity analysis

Mesh size and model parameters were calibrated, for each model separately, in an attempt to best reproduce the experimental load hydrograph (and in particular the peak load value) for the reference test case (h_u = 0.1 m). A sensitivity analysis was then performed to assess the influence of these parameters on the numerical predictions. This is actually a very useful information, especially in real field applications when reference data for calibration are not available. Some significant hydraulic quantities concerning the impact process were selected for the comparison.

For the 2D shallow water model, the influence of both the grid size and the Manning coefficient on the numerical results was investigated. In the reference simulation a grid size of 5 mm and a Manning coefficient of 0.007 s $m^{-1/3}$ were adopted. Numerical simulations with a coarser ($\Delta x = \Delta y$ = 12.5 mm) and with a finer ($\Delta x = \Delta y$ = 2.5 mm) mesh were carried out, maintaining the roughness coefficient equal to 0.007 s $m^{-1/3}$. The results of this sensitivity analysis are reported in Table 2. The results computed on the middle and on the finest grid differ by the order of 1%. This confirms that the grid size of 5 mm can be assumed as a reference, since a further refinement does not yield any substantial improvement of the numerical results. The calculated value of the peak impact force increases with the decreasing of the mesh size, and on the whole, it seems that the finest mesh predicts a more violent impact. However, the mesh size has no significant effect on the timing of the wave propagation during the initial stages of the dam-break and, consequently, the impact time. Table 3 shows the influence of the Manning coefficient n on the 2D numerical results if the

reference mesh of 5 mm is adopted. The rise in the value of the roughness parameter from 0.007 s $m^{-1/3}$ to 0.012 s $m^{-1/3}$ produces a reduction in the indicators of the impact strength (the peak load value decreases by about 4%) and an increase in the impact time value (by about 11%).

Table 2

Sensitivity of the 2D numerical results to the grid size for the reference test case (n = 0.007 s $m^{-1/3}$). Relative percent deviations are referred to the case with Δx = 2.5 mm (F_{max} = 6.80 N, t_{impact} = 0.356 s, I_{1s} = 3.39 N·s, I_{3s} = 13.72 N·s).

	F_{max}	t_{impact}	I_{1s}	I_{3s}
Δx = 5 mm	–0.90%	–0.59%	–1.73%	–0.68%
Δx = 12.5 mm	–3.90%	–0.36%	–6.89%	–3.48%

Table 3

Sensitivity of the 2D numerical results to the Manning coefficient for the reference test case (Δx = 5 mm). Relative percent deviations are referred to the case with n = 0.007 s $m^{-1/3}$ (F_{max} = 6.74 N, t_{impact} = 0.354 s, I_{1s} = 3.33 N·s, I_{3s} = 13.63 N·s).

	F_{max}	t_{impact}	I_{1s}	I_{3s}
n = 0.010 s $m^{-1/3}$	–2.73%	+7.07%	–4.78%	–2.64%
n = 0.012 s $m^{-1/3}$	–4.18%	+10.99%	–8.11%	–4.74%

Only a sensitivity analysis on mesh size and design was performed for the 3D Eulerian model. Three different mesh sizes were tested for the reference test case corresponding to mean element size of 30, 15, and 10 mm. Some significant results are reported in Table 4. If the largest mesh is used, the peak load is underestimated by about 12% with respect to the reference value obtained using the finest mesh, and the double-peak trend is not captured. On the other hand, the two finer meshes show almost identical results with regard to peak load and impulse. However, the finest mesh allows to better reproduce the experimental double-peak trend of the load time history (see, for example, the value of the local minimum occurring approximately at t = 0.9 s). Therefore, a 15 mm-mesh with a 10 mm-refinement around the obstacle was adopted to reduce the computational cost. Interestingly, the oscillations in the falling limb of the load hydrograph (see Fig. 10) appear only if the finest mesh is used. This is probably due to the fact that, after the first stages of the impact, a strong air-water mixing occurs in front of the obstacle. The VOF model takes this

effect into account by reducing the water volume fraction, which, in turn, affects the density and pressure fields. If a larger mesh is used, the air presence is distributed over larger volumes and becomes less important for the pressure field evaluation; in this way, fluctuations may not appear, but the flip-through type impact would not be reproduced as accurately.

Table 4

Sensitivity of the 3D finite volume results to the mean mesh size. Relative percent deviations are referred to the case with mean mesh size of 10 mm (F_{max} = 7.59 N, $F_{min\ (t\,=\,0.9\ s)}$ = 4.61 N, I_{1s} = 3.55 N·s).

Mean mesh size	F_{max}	$F_{min\ (t\,=\,0.9\ s)}$	I_{1s}
15 mm	–1.7%	+23.9%	–0.004%
30 mm	–11.7%	not detectable	–4.7%

SPH modelling required the definition of the particle resolution and the calibration of the artificial viscosity α introduced in Section 3.3. Three different values for each of these model parameters were considered for the sensitivity analysis. Table 5 reports some significant results obtained by setting the artificial viscosity equal to 0.15 and increasing the particle size from 2.5 to 5 to 10 mm. It can obviously be expected that the finest particle resolution is more suitable to accurately reproduce the dynamics of the impact process. On the other hand, the coarsest resolution leads to unsatisfactory results: the peak load and the impulse are exceedingly underestimated and the impact time is highly delayed if compared with the numerical predictions obtained on the basis of the reference finest resolution. Finally, 5 mm-resolution induces a noticeable overestimation of both impact force and long-time load impulse. Numerical SPH simulations with 2.5 mm particle resolution were performed assuming three different values for the artificial viscosity α (0.10, 0.15, and 0.20). The results are reported in Table 6. A slight decrease in the peak load and impulse is observed when α increases; instead, impact time is practically unaffected by this parameter. The value 0.15 was selected, being the minimum capable of guaranteeing numerical stability when impacts originated by higher values of the initial headwater h_u are modelled.

Table 5

Sensitivity of 3D SPH numerical results to particle resolution (α = 0.15). Relative percent deviations are referred to the case with particle size of 2.5 mm (F_{max} = 6.70 N, t_{impact} = 0.42 s, I_{1s} = 2.77 N·s, I_{3s} = 12.40 N·s).

Particle size	F_{max}	t_{impact}	I_{1s}	I_{3s}
5 mm	+22.54%	+16.67%	+2.53%	+18.31%
10 mm	–27.13%	+59.52%	–71.12%	–42.82%

Table 6

Sensitivity of 3D SPH numerical results to artificial viscosity (particle resolution of 2.5 mm). Relative percent deviations are referred to the case with α = 0.15 (F_{max} = 6.70 N, t_{impact} = 0.420 s, I_{1s} = 2.77 N·s, I_{3s} = 12.40 N·s).

α	F_{max}	t_{impact}	I_{1s}	I_{3s}
0.10	+11.19%	–4.76%	+8.30%	+3.23%
0.20	–2.39	+2.38%	–6.50%	–4.11%

It must be highlighted that all three models require an accurate spatial discretization of the computational domain to correctly reproduce the impact evolution, and this is particularly true for 3D models. In particular, the numerical results of the 3D Eulerian model appear to be fairly mesh design-dependent. However, if a detailed description of the impact evolution is not required, this model seems suitable for rough predictions of peak force and impulse, even when coarse meshes are used. The numerical results of the SPH model are strongly affected by artificial viscosity; the fact that this uncertain parameter is not physically based (and cannot be easily calibrated in the absence of reference data) tends to limit the predictive reliability of this model. Conversely, the 2D shallow water model appears to be less dependent on the Manning coefficient (chosen within a reasonable range of values), since the peak force and the impulse are estimated with only a few percent uncertainty.

4.5 Peak value of impact load

Peak impact force versus initial water depth within the reservoir is here analyzed. In this regard, in addition to the 40 runs performed for the initial headwater of 0.10 m, a set of 5 runs was also carried out for 12 additional initial still-water depths in the reservoir (ranging from 0.07 m to 0.13 m with 5 mm step). All the peak load measurements were statistically processed by joining each value – normalized by the sample mean estimate of the corresponding homogeneous group – into a single big sample of approximately one hundred elements. Extending the results of the repeatability analysis discussed in Section 4.2, it was assumed that this large dimensionless sample was normally distributed too. Moreover, the

value of the coefficient of variation calculated for this sample was considered a reliable estimate of the variability of all the original dimensional data sets. This allowed to attribute a confidence interval based on Gaussian distribution to the maximum impact load estimation for each headwater value considered.

Fig. 12a shows the comparison between experimental measurements and numerical results. Gray vertical bars indicate the 90% confidence interval between 5% and 95% percentile levels calculated from the observed data on the basis of the assumptions previously described.

A quadratic relationship between the two variables seems to occur in the range of h_u considered. Indeed, both experimental and numerical data fit well with second degree polynomial curves (shown in Fig. 12b) characterized by a coefficient of determination which, in the worst case, is equal to 0.9966. This quadratic dependence is consistent with the outcome of a simplified one-dimensional theoretical analysis based on the hypothesis that both the propagation of the dam-break wave in the first stages and the formation of the vertical bulge at the wall are not affected by energy dissipation (see [3]). If the velocity of the wetting front is assumed to be proportional to $h_u^{1/2}$ (as in the Ritter problem), the application of the Bernoulli theorem ensures that the maximum height of the vertical jet is a multiple of h_u. The corresponding maximum impact force is a function of h_u^2, if a hydrostatic pressure distribution is assumed. An improved analysis could take into account unsteady and two-dimensional effects.

For lower values of h_u (< 0.09 m), all the numerical models overestimate the peak load experimental data introducing an error of few percent. In the remaining range of h_u, 3D numerical predictions are very close to (and even fall into) the 90% confidence interval of the observed data with the exception of the SPH model, which shows a significant overestimation of the peak load for the highest headwater depths investigated (h_u > 0.12 m). The 2D shallow water numerical model instead underestimates the peak load values for h_u > 0.09 m with a relative error in the order of 10%.

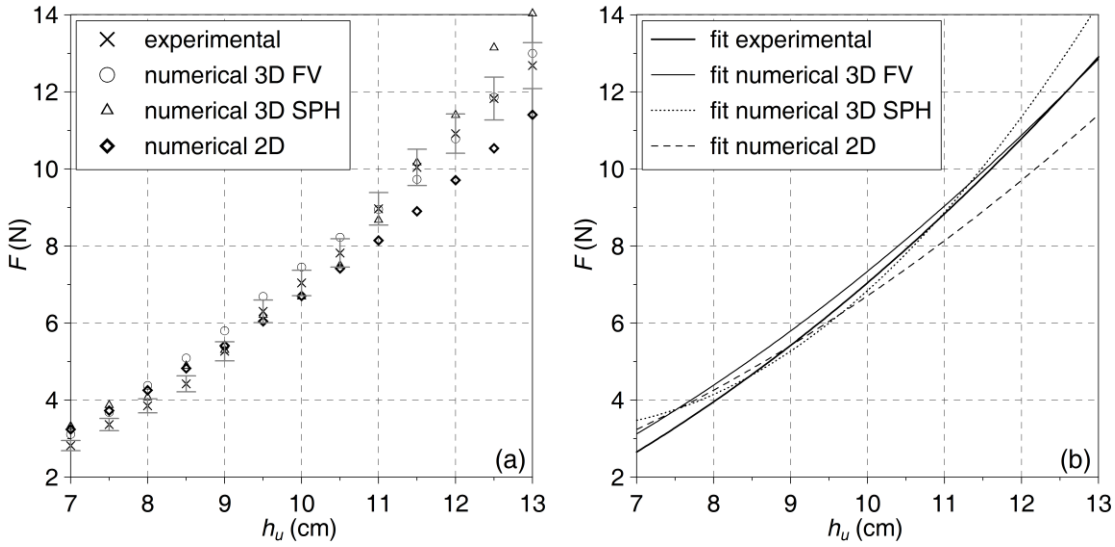

Fig. 12. Impact peak force versus initial water depth within the reservoir. (a) Comparison between measured data and numerical results; gray bars indicate the estimated 90% confidence interval of the observed data based on Gaussian distribution. (b) Comparison between experimental and numerical least-square fitting curves based on second degree polynomials.

5 Conclusions

Measured impact force shows remarkable variability under the same initial test conditions, and therefore a statistical analysis provides useful information about the values of maximum impact forces of different probabilities. Load impulse, instead, shows greater consistency in characterizing wave impact.

The analysis of the experimental relationship between peak impact force and initial water depth upstream of the dam shows a quadratic dependence in the range here examined. This behaviour is consistent with a simplified theoretical description of the impact based on the inviscid flow approximation.

Once successfully calibrated with respect to a reference test case, the 2D and 3D models used in this work are able to reproduce the trend of increasing peak impact force with increasing initial headwater depth. In particular, the 3D models provide an accurate prediction of the peak load values, even if the SPH model is rather precautionary, especially for more violent impact events. Anyway, the 3D models are able to describe the main characteristics of the complex dynamics of the flip-through impact process and capture the impact loading time histories for the test cases considered, but at the price of computationally demanding numerical simulations and a considerable preliminary effort for the mesh design and the model calibration. The adoption of a two-phase model seems to improve the capability of the numerical simulations to reproduce the first stages of the impact and capture the load peak

values, even if the wave dynamics after the secondary peak is not correctly reproduced by FLUENT, which overestimates the falling limb of the load hydrograph with noticeable mesh-dependent fluctuations.

On the other hand, because of the importance of three-dimensional effects in impact-type phenomena, the 2D shallow water model is not as accurate in predicting the force time series recorded. In particular, this approach overestimates long time load impulse, thus tending to provide an overestimation of the linear momentum transmitted to the structure over long time durations. Similar behaviour for this integral property is predicted by FLUENT. Impact peak load is underestimated by the 2D shallow water model with an error in the order of only 10%, which might be considered acceptable in relation with the various sources of uncertainty involved in this kind of problems and in consideration of the fact that the failure point of structures cannot usually be predicted with comparable accuracy. However, when the shallow water approximation is expected to work well (for lower initial water depths in the upstream reservoir), 2D results are totally comparable with the experimental data, as well as with the numerical predictions of far more sophisticated and computational demanding 3D solvers.

The predictive capability of the 3D finite volume solver is fairly mesh-design dependent and considerably influenced by the average mesh size: if spatial resolution is not sufficiently high, the double-peak trend shown by the observed impact load hydrograph cannot be reproduced. The SPH solver seems more accurate in reproducing longer time evolution of load impulse, even though it handles only one-phase free surface flows. However, the SPH model is rather sensitive to particle resolution and artificial viscosity, and requires a very small particle size to reproduce experimental load data accurately. The sensitivity analysis accomplished on the 2D shallow water model shows that, on the whole, a decrease in the grid size or in the roughness induces the prediction of a more violent impact. Both peak impact force and impulse load are estimated with some percent uncertainty due to model sensitivity to these parameters. Since the 2D shallow water approach is widely used in large scale real field applications (often being the only one really adoptable in these situations from a computational point of view) the awareness of the extent of all these performances can be of help for a proficient use of this kind of modelling, especially when calibration data are not available.

Finally, the experimental data collected can provide a good benchmark for validating numerical models and are available online to the user community as supplementary material.

Acknowledgements

The reviewers are kindly acknowledged for their valuable comments, which have greatly contributed to the improvement of the paper. The Italian interuniversity consortium CINECA is also acknowledged for the availability of high performance computing resources.

Supplementary material

- File F1. Video of a typical experimental run (in MP4 format); the still frames reported in Fig. 2 are captured from this video.
- File F2. Experimental load and impulse time series represented in Figs. 10 and 11 (in TXT format).
- File F3. Experimental data concerning impact peak force shown in Fig. 12 (in TXT format).

References

[1] Abdolmaleki K, Thiagarajan KP, Morris-Thomas MT. Simulation of the dam break problem and impact flows using a Navier-Stokes solver. Proc. 15th Australasian Fluid Mechanics Conf. 2004; Sydney, Australia, M. Behnia, W. Lin, G.D. McBain, eds. Curran Associates, New York.

[2] Altomare C, Crespo AJC, Rogers BD, Domínguez JM, Gironella X, Gómez-Gesteira M. Numerical modelling of armour block sea breakwater with Smoothed Particle Hydrodynamics, Comput Struct 2014;130:34–45.

[3] Armanini A, Larcher M, Odorizzi M. Dynamic impact of a debris flow front against an obstacle. Proc. 5th Int. Conf. on Debris Flow Hazards. Mitigation, mechanics, prediction and assessment 2011, Padua, Italy; R. Genevois, D. L. Hamilton, A. Prestininzi, eds. Casa Editrice Università La Sapienza, Rome.

[4] Aureli F, Maranzoni A, Mignosa P, Ziveri C. Flood hazard mapping by means of fully-2D and quasi-2D numerical modeling: a case study. Proc. 3rd Int. Symposium on Flood Defence 2006, Nijmegen, The Netherlands; J. van Alphen, E. van Beek, M. Taal, eds. Taylor & Francis, Leiden.

[5] Aureli F, Maranzoni A, Mignosa P, Ziveri C. Dam-break flows: acquisition of experimental data through an imaging technique and 2D numerical modeling. J Hydraulic Eng 2008;134(8),1089–1101.

[6] Aureli F, Maranzoni A, Mignosa P, Ziveri C. 2D numerical modeling for hydraulic hazard assessment: a dam-break case study. Proc. Int. Conf. River Flow 2008; Lisbon,

Portugal, Vol. 1, 729–736, M. Altinakar, M.A. Kokpinar, I. Aydin, S. Cokgor, S. Kirkgoz, eds. Kubaba Congress Department and Travel Services, Ankara, Turkey.

[7] Aureli F, Maranzoni A, Mignosa P, Ziveri C. A weighted surface-depth gradient method for the numerical integration of the 2D shallow water equations with topography. Adv Water Res 2008;31(7),962–974.

[8] Barreiro A, Crespo AJC, Domínguez JM, Gómez-Gesteira M. Smoothed Particle Hydrodynamics for coastal engineering problems. Comput Struct 2013;120(15),96–106.

[9] Begnudelli L, Sanders BF. Simulation of the St. Francis dam-break flood. J Eng Mech 2007;133(11),1200–1212.

[10] Braschi G, Gallati M. Simulation of a levee-breaking submersion of planes and urban areas. Proc. HYDROCOMP '89, Int. Conf. on computational modelling and experimental methods in Hydraulics 1989; Dubrovnik, Yugoslavia, 117–126, Elsevier Applied Sciences, London.

[11] Bredmose H, Hunt-Raby A, Jayaratne R, Bullock GN. The ideal flip-through impact: experimental and numerical investigation. J Eng Math 2010;67:115–136.

[12] Bukreev VI, Zykov VV. Bore impact on a vertical plate. J Appl Mech Techn Phys 2008;49(6),926–933.

[13] Bukreev VI. Force action of discontinuous waves on a vertical wall. J Appl Mech Techn Phys 2009;50(2),278–283.

[14] Bullock GN, Obhrai C, Peregrine DH, Bredmose H. Violent breaking wave impacts. Part 1: results from large-scale regular wave tests on vertical and sloping walls. Coastal Eng 2007; 54,602–617.

[15] Chan ES, Cheong HF, Tan BC. Laboratory study of plunging wave impacts on vertical cilinders. Coastal Eng 1995;25,87–107.

[16] Chen HY, Xu WL, Deng J, Xue Y, Li J. Experimental investigation of pressure load exerted on a downstream dam by dam-break flow. J Hydraulic Eng 2014;140(2),199–207.

[17] Colagrossi A, Landrini M. Numerical simulation of interfacial flows by smoothed particle hydrodynamics. J Comput Phys 2003;191(2),448–475.

[18] Colagrossi A, Colicchio G, Lugni C, Brocchini M. A study of violent sloshing wave impacts using an improved SPH method. J Hydraulic Res 2010;48(Supplement 1),94–104.

[19] Cooker MJ, Peregrine DH. Computation of violent wave motion due to waves breaking against a wall. Proc. 22nd Int. Conf. on Coastal Engineering 1990; Delft, The Netherlands, 164–176, ASCE, New York.

[20] Cummins SJ, Silvester TB, Cleary PW. Three-dimensional wave impact on a rigid structure using smoothed particle hydrodynamics. Int J Numer Meth Fluids 2012;68,1471–1496.

[21] Cuomo G, Allsop W, Bruce T, Pearson J. Breaking wave loads at vertical seawalls and breakwaters. Coastal Eng 2010;57,424–439.

[22] Doebelin EO. Measurement systems. Application and design. McGraw-Hill, New York; 1990.

[23] Erpicum S, Archambeau P, Dewals BJ, Ernst J, Pirotton M. Dam-break flow numerical modeling considering structural impacts on buildings. Proc. 33rd IAHR Congress 2009; Vancouver, Canada, 3951–3958.

[24] European Council (2007). EU Flood Directive 2007/60.

[25] Ferrari A, Dumbser M, Toro EF, Armanini A. A new 3D parallel SPH scheme for free surface flows. Computers & Fluids 2009;38,1203–1217.

[26] FLUENT. Fluent 14.0 User's Guide 2011. ANSYS Inc., software documentation.

[27] Gallegos HA, Schubert JE, Sanders BF. Structural damage prediction in a high-velocity urban dam-break flood: field-scale assessment of predictive skill. J Eng Mech 2012;138(10),1249–1262.

[28] Gómez-Gesteira M, Dalrymple RA. Using a three-dimensional smoothed particle hydrodynamics method for wave impact on a tall structure. J Waterw Port Coastal Ocean Eng 2004;130(2),63–69.

[29] Gómez-Gesteira M, Rogers BD, Dalrymple RA, Crespo AJC. State of the art of classical SPH for free-surface flows. J Hydraulic Res 2010;48(Supplement 1),6–27.

[30] Gómez-Gesteira M, Rogers BD, Crespo AJC, Dalrymple RA, Narayanaswamy M, Dominguez JM. SPHysics - development of a free-surface fluid solver- Part 1: Theory and Formulations. Computers & Geosciences 2012;48,289–299.

[31] Hattori M, Arami A, Yui T. Wave impact pressure on vertical walls under breaking waves of various type. Coastal Eng1994;22,79–114.

[32] Hervouet JM, Petitjean A. Malpasset dam-break revisited with two-dimensional computations. J Hydraulic Res 2006;37(6),377–388.

[33] Hirt CW, Nichols BD. Volume of fluid (VOF) method for the dynamics of free boundaries. J Comput Phys 1981;39(1),201–225.

[34] Hughes J, Graham D. Comparison of incompressible and weakly-compressible SPH models for free-surface water flows. J Hydraulic Res 2010;48(Supplement 1),105–117.

[35] Kelman I, Spence R. An overview of flood actions on buildings. Eng Geol 2004;73,297–309.

[36] Kirkgöz MS. Breaking wave impact on vertical and sloping coastal structures. Ocean Eng 1994;22(1),35–48.

[37] Kleefsman KMT, Fekken G, Veldman AEP, Iwanowski B, Buchner B. A Volume-of Fluid based simulation method for wave impact problems. J Comput Phys 2005;206(1),363–393.

[38] LaRocque LA, Imran J, Chaudhry MH. 3D numerical simulation of partial breach dam-break flow using the LES and *k-ε* turbulence models. J Hydraulic Res 2013;51(2),145–157.

[39] Lauber G, Hager WH. Experiments to dambreak wave: horizontal channel. J Hydraulic Res 1998;36(3),291–307.

[40] Li S, Liu WK. Smoothed Particle Hydrodynamics. World Scientific Publishing, Singapore; 2003.

[41] Lobovský L, Botia-Vera E, Castellana F, Mas-Soler J, Souto-Iglesias A. Experimental investigation of dynamic pressure loads during dam-break. J Fluids Struct 2014;48, 407–434.

[42] Lugni C, Brocchini M. Faltinsen OM. Wave impact loads: the role of the flip-through, Phys Fluids 2006;18(12):122101.

[43] Lugni C, Miozzi M, Brocchini M, Faltinsen OM. Evolution of the air cavity during a depressurized wave impact. I. The kinematic flow field, Phys Fluids 2010;22(5):056101.

[44] Lugni C, Brocchini M, Faltinsen OM. Evolution of the air cavity during a depressurized wave impact. II. The dynamic field, Phys Fluids 2010; 22(5):056102.

[45] Marrone S, Antuono M, Colagrossi A, Colicchio G, Le Touzé D, Graziani D.. δ-SPH model for simulating violent impact flows. Comput Method Appl M 2011;200(13–16),1526–1542.

[46] Monaghan JJ. Smoothed particle hydrodynamics. Reports on Progress in Physics 2005;68,1703–1759.

[47] Monaghan JJ, Kos A. Solitary waves on a Cretan beach. J Waterw Port Coastal Ocean Eng 1999;125(3),145–155.

[48] Morris JP, Fox PJ, Zhu Y. Modelling low Reynolds number incompressible flows using SPH, J Comput Phys 1997;136,214–226.

[49] Peregrine DH. Water-wave impact on walls. Ann Rev Fluid Mech 2003;35,23–43.

[50] Raad PE, Bidoae R. The three-dimensional Eulerian-Lagrangian marker and micro cell method for the simulation of free surface flows. J Comput Phys 2005;203(2),668–699.

[51] Ramsden JD, Raichlen F. Forces on vertical wall caused by incident bores. J Waterw Port Coastal Ocean Eng 1990;116(5),592–613.

[52] Ramsden JD. Forces on a vertical wall due to long waves, bores, and dry-bed surges. J Waterw Port Coastal Ocean Eng 1996;122(3),134–141.

[53] RESCDAM. Development of rescue action based on dam-break flood analysis. The use of physical models in dam-break flood analysis. Final report, Helsinki Univ. of Technology, Helsinki, Finland; 2000.

[54] Sanders BF, Schubert JE, Gallegos HA. Integral formulation of shallow-water equations with anisotropic porosity for urban flood modeling. J Hydrology 2008;362(1–2),19–38.

[55] Shige-eda M, Akiyama J. Numerical and experimental study on two-dimensional flood flows with and without structures. J Hydraulic Eng 2003;129(10),817–821.

[56] Schubert JE, Sanders BF. Building treatments for urban flood inundation models and implications for predictive skill and modeling efficiency. Adv Water Res 2012; 41:49–64.

[57] Soares Frazão S, Zech Y. Experimental study of dam-break flow against an isolated obstacle. J Hydraulic Res 2007;45(Extra Issue),27–36.

[58] Soares Frazão S, Zech Y. Dam-break flow through an idealised city. J Hydraulic Res 2008;46(5),648–658.

[59] Soares Frazão S, Lhomme J, Guinot V, Zech Y. Two-dimensional shallow-water model with porosity for urban flood modelling. J Hydraulic Res 2008;46(1),45–64.

[60] Tanrikulu AK, Kirkgöz MS, Dündar C. Theoretical and experimental investigation of a vertical wall response to wave impact. Ocean Eng 2002;29,769–782.

[61] Thieken AH, Muller M, Kreibich H, Merz B. Flood damage and influencing factors: new insights from the August 2002 flood in Germany. Water Resour Res 2005;41,W12430.

[62] Thusyanthan NI, Madabhushi SPG. Tsunami wave loading on coastal houses: a model approach. Proc. of ICE, Civil Engineering 2008;161,77–86.

[63] Toro EF. Shock-capturing methods for free-surface shallow flows. John Wiley & Sons, Chichester, England; 2001.

[64] Trivellato F. Hydrodynamic forces due to the impact of a water bore on a structure. Transactions on the Built Environment 2001;56,25–34.

[65] Trivellato F. Experimental and numerical investigation of bore impact on a wall. Transactions on the Built Environment 2004;71,3–12.

[66] Vacondio R, Rogers BD, Stansby PK, Mignosa P. A correction for balancing discontinuous bed slopes in two-dimensional smoothed particle hydrodynamics shallow water modeling. Int J Numer Meth Fluids 2012;71:850–872.

[67] Vacondio R, Rogers BD, Stansby PK, Mignosa P. Shallow water SPH for flooding with dynamic particle coalescing and splitting. Adv Water Res 2013;58,10–23.

[68] Vacondio R, Mignosa P, Pagani S. 3D SPH numerical simulation of the wave generated by the Vajont rockslide, Adv Water Res 2013;59,146–156.

[69] Violeau D, Leroy A. On the maximum time step in weakly compressible SPH. J Comput Phys 2014;256,388–415.

[70] Yang C, Lin B, Jiang C, Liu Y. Predicting near-field dam-break flow and impact force using a 3D model. J Hydraulic Res 2010;48(6),784–792.

[71] Zanuttigh B, Lamberti A. Experimental analysis of the impact of dry avalanches on structures and implication for debris flows. J Hydraulic Res 2006;44(4),522–534.